Accepted for publication in the Astrophysical Journal
Preprint typeset using LaTeX style emulateapj v. 5/2/11

arXiv:1207.0518v1 [astro-ph.SR] 2 Jul 2012

GERMANIUM, ARSENIC, AND SELENIUM ABUNDANCES IN METAL-POOR STARS[1]

Ian U. Roederer
Carnegie Observatories, 813 Santa Barbara Street, Pasadena, CA 91101, USA

Accepted for publication in the Astrophysical Journal

ABSTRACT

The elements germanium (Ge, $Z = 32$), arsenic (As, $Z = 33$), and selenium (Se, $Z = 34$) span the transition from charged-particle or explosive synthesis of the iron-group elements to neutron-capture synthesis of heavier elements. Among these three elements, only the chemical evolution of germanium has been studied previously. Here we use archive observations made with the Space Telescope Imaging Spectrograph on board the *Hubble Space Telescope* and observations from several ground-based facilities to study the chemical enrichment histories of seven stars with metallicities $-2.6 \leq$ [Fe/H] ≤ -0.4. We perform a standard abundance analysis of germanium, arsenic, selenium, and several other elements produced by neutron-capture reactions. When combined with previous derivations of germanium abundances in metal-poor stars, our sample reveals an increase in the [Ge/Fe] ratios at higher metallicities. This could mark the onset of the weak *s*-process contribution to germanium. In contrast, the [As/Fe] and [Se/Fe] ratios remain roughly constant. These data do not directly indicate the origin of germanium, arsenic, and selenium at low metallicity, but they suggest that the weak and main components of the *s*-process are not likely sources.

Subject headings: nuclear reactions, nucleosynthesis, abundances — stars: abundances — stars: individual (HD 2454, HD 16220, HD 76932, HD 94028, HD 107113, HD 140283, HD 160617)

1. INTRODUCTION

An incomplete but nevertheless intriguing history of stellar nucleosynthesis may be reconstructed from the abundance patterns revealed by the heavy elements present today. The atmospheres of cool stars largely preserve the initial chemical composition of the interstellar medium (ISM) at the time and place where each star formed. Neutral and singly-ionized atoms, the majority species in these atmospheres, absorb radiation at energies in the optical spectrum accessible to ground-based telescopes. These favorable conditions allow us to study the chemical record in the Sun and other stars whose ages span the full age of the Universe.

We can interpret the origin of elements that are readily detected in these stars with the help of models of stellar structure and chemical evolution, as well as steadily growing volumes of laboratory atomic and nuclear physics data. For example, substantial fractions of the iron-group elements in the Solar system were produced under explosive conditions in equilibrium or quasi-equilibrium during previous generations of supernovae. The overwhelming majority of the Solar composition of significantly heavier elements, such as barium (Ba, $Z = 56$) or europium (Eu, $Z = 63$), must have been produced by neutron-capture (n,γ) reactions and subsequent β^{-} decays. Insurmountable Coulomb barriers prevent charged-particle reactions from contributing all but a negligible fraction of such elements. Elements between these two extremes, such as strontium (Sr, $Z = 38$) or zirconium (Zr, $Z = 40$), may be produced by each of these mechanisms.

Elements in this transition between zinc (Zn, $Z = 30$) and rubidium (Rb, $Z = 37$) are rarely studied in late-type stars because their intrinsic abundances are relatively low and their strongest absorption lines lie in the ultraviolet (UV), below the atmospheric cutoff near 3000 Å. Some of these intermediate elements have been detected in the atmospheres of so-called chemically-peculiar stars (e.g., Bidelman & Corliss 1962; Leckrone et al. 1999; Castelli & Hubrig 2004; Cowley et al. 2010). These atmospheres are affected by strong magnetic fields or are stable against convection, allowing radiatively driven diffusion or gravitational settling to chemically stratify the atmosphere. These stars are not useful records for examining the evolution of specific elements throughout the history of the Galaxy. Gallium (Ga, $Z = 31$) has been detected in just a few unstratified stars by Ivans et al. (2003, 2006). Several high ionization states of some of these elements are found in planetary nebulae (e.g., Péquignot & Baluteau 1994; Dinerstein 2001; Sterling et al. 2002; Sharpee et al.

---

iur@obs.carnegiescience.edu

[1] Based on observations made with the NASA/ESA *Hubble Space Telescope*, obtained from the data archive at the Space Telescope Science Institute. STScI is operated by the Association of Universities for Research in Astronomy, Inc. under NASA contract NAS 5-26555. This research made use of StarCAT, hosted by the Mikulski Archive at the Space Telescope Science Institute (MAST). These data are associated with Programs GO-7348, GO-7433, GO-8197, GO-9048, GO-9455, and GO-9804.

Based on data obtained from the European Southern Observatory (ESO) Science Archive Facility. These data are associated with Programs 67.D-0439(A), 074.C-0364(A), 076.B-0055(A), and 080.D-0347(A).

This research has made use of the Keck Observatory Archive (KOA), which is operated by the W.M. Keck Observatory and the NASA Exoplanet Science Institute (NExScI), under contract with the National Aeronautics and Space Administration. These data are associated with Programs H2aH, H6aH, and H39aH (P.I. Boesgaard), N01H (P.I. Latham), and U11H (P.I. Prochaska).

This paper includes data taken at The McDonald Observatory of The University of Texas at Austin.

2007; Sterling & Dinerstein 2008). Recent work by Karakas et al. (2007, 2009) interprets these abundances in terms of self-enrichment by the slow neutron capture process (*s*-process). This process operates in intermediate-mass stars during the asymptotic giant branch (AGB) phase of evolution, which precedes the planetary nebula stage. Some of these elements are also detected in the ISM of the Milky Way (e.g., Pwa & Pottasch 1986; Cardelli et al. 1991; Hobbs et al. 1993) or other galaxies at high redshift (e.g., Prochaska et al. 2003). While general conclusions can be made, it is difficult to probe stellar nucleosynthesis using the integrated heavy elements found in this gas at the level of detail afforded by individual stars in our own Galaxy.

Among the elements between zinc and rubidium, only germanium (Ge, $Z = 32$) has been examined in more than a handful of late-type stars (Sneden et al. 1998, 2003; Cowan et al. 2002, 2005; Roederer et al. 2012). Yet even this sample comprises only old halo stars with metallicity [Fe/H] < -1.4, so the evolution of germanium in younger disc stars with higher metallicity is still unknown. Recently, Roederer & Lawler (2012) detected neutral arsenic (As, $Z = 33$) and selenium (Se, $Z = 34$) in the metal-poor halo star HD 160617 using a high-resolution UV spectrum obtained with the Space Telescope Imaging Spectrograph (STIS) on board the *Hubble Space Telescope* (*HST*). That study was able to place an interesting upper limit on the germanium abundance through the non-detection of Ge i. With the exception of one good Ge i absorption line at 3039 Å, the only detectable transitions of these elements lie near 2000 Å in the UV. No ground-based telescope offers the opportunity to study all three of these elements simultaneously.

We have searched the *HST* archives to find any stellar spectra that offer a reasonable opportunity to detect the rarely-studied elements germanium, arsenic, and selenium. We find suitable spectra of six stars that span a range of metallicities and stellar populations. We summarize some relevant properties of these elements in Section 2, characterize the archival observations in Section 3, describe our analysis in 4, present our results in Section 5, and summarize our conclusions in Section 6.

Throughout this work we use standard definitions of elemental abundances and ratios. For element X, the abundance is defined as the logarithm of the number of atoms of element X per 10^{12} hydrogen atoms, $\log\epsilon(\mathrm{X}) \equiv \log_{10}(N_\mathrm{X}/N_\mathrm{H}) + 12.0$. For elements X and Y, the abundance ratio relative to the solar ratio of X and Y is defined as the logarithm $[\mathrm{X/Y}] \equiv \log_{10}(N_\mathrm{X}/N_\mathrm{Y}) - \log_{10}(N_\mathrm{X}/N_\mathrm{Y})_\odot$. Abundance ratios, e.g., [X/Fe], are constructed by comparing the total abundance of element X derived from the neutral species with the total iron abundance derived from Fe i or the total abundance of element X derived from the ionized species with the total iron abundance derived from Fe ii. Abundances or ratios denoted with the ionization state indicate the particular ionization state used to derive the total number of atoms of the element under consideration.

2. GERMANIUM, ARSENIC, AND SELENIUM IN THE SOLAR SYSTEM

Five isotopes of germanium occur naturally in the Solar system, ^{70,72,73,74,76}Ge. The lightest four of these isotopes are accessible to the *s*-process, and even ^{76}Ge may be accessible to the *s*-process if the branching point at ^{75}Ge is open. All but ^{70}Ge are accessible to the rapid (*r*) neutron-capture process. Only one isotope of arsenic is found in Solar material, ^{75}As, which may be produced by both *s*- and *r*-process nucleosynthesis. There are six naturally-occurring isotopes of selenium, ^{74,76,77,78,80,82}Se. Four of these isotopes, ^{76,77,78,80}Se, lie along the *s*-process chain, and only ^{74}Se and ^{76}Se are shielded from the *r*-process. ^{74}Se may be produced by proton-capture (p,γ) or other reactions that produce nuclei on the proton-rich side of stability. ^{74}Se constitutes only a minor fraction (0.89%) of the total elemental abundance, and we shall not consider it further here. The Solar isotopic abundances of these three elements are well-known and are summarized in, e.g., Böhlke et al. (2005).

Several of the heavier isotopes of selenium derive a large fraction of their Solar abundance from the *r*-process production of radioactive isotopes with 50 neutrons. This stable nuclear configuration gives rise to smaller than average cross sections to neutron capture reactions, building up a peak in the *r*-process distribution. After the *r*-process shuts off, these radioactive isotopes β^- decay to stable isotopes of selenium. Selenium is unique among the elements in our study because it lies at the first *r*-process peak. Similar phenomena occur in nuclei with 82 and 126 neutrons, the second and third peaks, respectively.

The classical approach to calculating the *r*-process contribution to the Solar abundance distribution, $N_r = N_\odot - N_s$, neglects to account for the multitude of nucleosynthesis channels that can produce elements between the iron-group and the first *s*-process peak (krypton through zirconium, $36 \leq Z \leq 40$). These decompositions assigned a very large *s*-process fraction (∼20–70%) to the Solar germanium, arsenic, and selenium abundances (e.g., Käppeler et al. 1982 or Burris et al. 2000; see Cameron 1982 for a similar approach). Modern decompositions using the stellar model approach of Gallino et al. (1998), Arlandini et al. (1999), and the updates given in Bisterzo et al. (2011) assign only 5–10% of the Solar abundances of germanium, arsenic, and selenium to the main component of the *s*-process. The *p*-process contributions to the Solar abundances are expected to be quite small (e.g., Käppeler et al.). The remainder is assumed to originate in the weak component of the *s*-process or mechanisms associated with core-collapse supernovae. Pignatari et al. (2010) estimate the primary, or explosive, component of the Solar germanium abundance to be 5–8%. Applying a model of Galactic chemical evolution, Travaglio et al. (2004a) estimate another 12% of the Solar germanium should originate in low-mass stars passing through the AGB phase. Type Ia supernovae should produce no significant germanium (e.g., Travaglio et al. 2004b). The remaining 80% of the Solar abundance of germanium should be produced by the weak *s*-process operating in massive stars (e.g., Pignatari et al.). Regardless of the exact fractions, modern methods of accounting for the various nucleosynthesis contributions make clear that the main *s*-process component had a relatively minor influence on the total Solar abundances of these elements.

3. OBSERVATIONS FROM THE ARCHIVES

We have searched the *HST* archives to find high-resolution spectral observations covering wavelengths from $1890 \leq \lambda \leq 2074$ Å where Ge I, As I, and Se I lines may be found. The archive contains six subgiants with adequate signal-to-noise (S/N) ratios (S/N $\gtrsim$ 20 near 2000 Å) and similar stellar parameters: HD 2454, HD 16220, HD 76932, HD 94028, HD 107113, and HD 140283. Roederer & Lawler (2012) also studied these elements in an archival STIS spectrum of another star, HD 160617. These stars comprise our target sample for the present study.

All UV spectra were taken with STIS (Kimble et al. 1998; Woodgate et al. 1998). These spectra were obtained using either the high resolution E230H grating or the medium resolution E230M grating. Table 1 reports the details of each set of observations, including wavelength coverage, exposure time, approximate spectral resolution, S/N ratios at a few reference wavelengths, program identifier, and the principle investigator (P.I.) of the original observations. We use the reduction and coaddition provided by the StarCAT database (Ayres 2010).

These are local ($20 < d < 60$ pc), bright stars ($5.8 < V < 8.7$), and they have been observed many times using ground-based instruments. We supplement the UV spectra with optical spectra obtained with the High Accuracy Radial velocity Planet Searcher (HARPS; Mayor et al. 2003) on the ESO 3.6 m Telescope at La Silla, Chile; the Ultraviolet and Visual Echelle Spectrograph (UVES; Dekker et al. 2000) on the Very Large Telescope (VLT) Kueyen at Cerro Paranal, Chile; and the High Resolution Echelle Spectrometer (HIRES; Vogt et al. 1994) on the Keck I Telescope at Mauna Kea, Hawai'i. These spectra were reduced and extracted using the standard instrument pipelines, and we performed the final processing within the IRAF environment. New observations of HD 94028 were obtained on 2009 February 18 and 2009 June 12 using the Robert G. Tull Coudé Spectrograph (Tull et al. 1995) on the 2.7 m Harlan J. Smith Telescope at McDonald Observatory, Texas. These data were reduced and combined using the REDUCE software package (Piskunov & Valenti 2002) and standard IRAF procedures. We use this spectrum to supplement the HIRES spectrum of HD 94028 at longer wavelengths. The details of each of these observations are also listed in Table 1. Our previous study of HD 160617 revealed no systematic differences at the 1 mÅ level between sets of equivalent widths (EWs) measured from high-quality spectra collected with these instruments.

4. ABUNDANCE ANALYSIS

4.1. *Model Atmospheres*

We interpolate model atmospheres from the ATLAS9 grid of Castelli & Kurucz (2003), using the α-enhanced grid for stars with overall metallicity [Fe/H] < -0.7. We use the latest version of the analysis code MOOG (Sneden 1973), including updates from Sobeck et al. (2011), to perform a standard EW abundance analysis for iron. We measure EWs of Fe I and Fe II lines using a semi-automated routine that fits Voigt absorption line profiles to continuum-normalized spectra. We adopt the log(gf) values for Fe I and Fe II lines from the critical compilation of Fuhr & Wiese (2006). We adopt damping constants from Barklem et al. (2000) and Barklem & Aspelund-Johansson (2005), when available, and otherwise we resort to the standard Unsöld (1955) approximation. We calculate surface gravities, log g (cm s^{-2}), based on the *Hipparcos* parallax measurements validated by van Leeuwen (2007), bolometric corrections from Alonso et al. (1999), stellar masses from Casagrande et al. (2011), and Solar parameters $M_{\rm bol} = 4.74$, log $g_{\odot} = 4.44$, and $T_{\rm eff\odot} = 5780$ K. We derive effective temperatures, $T_{\rm eff}$, by requiring that the abundances derived from individual Fe I lines show no dependence on lower excitation potential (E.P.). We derive microturbulent velocities, $v_{\rm t}$, by requiring that these abundances show no trend with line strength. We set the overall metallicity of the model atmosphere equal to the iron abundance derived from Fe II. Reddening along the line of sight to these stars is insignificant and can be neglected (e.g., Casagrande et al.). We iterate on the model atmosphere parameters until reaching convergence, which typically requires 2–4 iterations.

Our derived model atmosphere parameters and iron abundances are listed in Table 2. Uncertainties in the atmospheric parameters should be comparable to those discussed in Section 4.1 of Roederer & Lawler (2012). Our derived temperatures are consistently several hundred K cooler than temperatures calculated using color-temperature relations or the infrared flux method. The warmer temperature scales all introduce a correlation between E.P. and abundance, signaling the need for a cooler temperature scale. This is not ideal, but other approaches (e.g., Balmer line profiles, color-temperature relations) also incur difficulties. Absolute abundances should be viewed with caution. Since all of our stars are subgiants or turn-off stars with similar temperatures, the abundance ratios of one heavy element to another should be affected minimally.

4.2. *Derivation of Abundances*

Our techniques are the same as those employed by Roederer & Lawler (2012). We derive all heavy element abundances by comparing synthetic spectra, computed using MOOG, with the observed spectrum. Syntheses of several lines in HD 140283 are shown in Figure 1 as examples. Lines of other species near those of interest are synthesized based on the Kurucz & Bell (1995) line lists, updating their log(gf) values with more recent laboratory or theoretical values when available. These lines have already been discussed by Roederer & Lawler. In addition to germanium, arsenic, and selenium, we also derive abundances of a selection of heavier elements useful for interpreting the enrichment history of these stars: zinc, strontium, zirconium, barium, lanthanum (La, $Z = 57$), europium, platinum (Pt, $Z = 78$), and lead (Pb, $Z = 82$). In all cases, we adopt the Solar abundances from Asplund et al. (2009): iron, $\log\epsilon = 7.50$; zinc, 4.56; germanium, 3.65; arsenic, 2.30; selenium, 3.34; strontium, 2.87; zirconium, 2.58; barium, 2.18; lanthanum, 1.10; europium, 0.52; platinum, 1.62; and lead, 2.04.

Table 3 lists the 49 lines we have examined. We adopt the log(gf) values for Zn I and II, As I, and Pt I from Roederer & Lawler (2012); Ge I, Sr II, and Ba II from the NIST critical compilations (Klose 2002; Fuhr & Wiese 2009); Se I from Morton (2000); Zr II

TABLE 1
Characteristics of the Archival Spectra

Star	λ (Å)	Instrument	$t_{\rm exp}$ (s)	$R \equiv \lambda/\Delta\lambda$	S/N @ λ	Program	P.I.
HD 2454	1970–2770	STIS	1929	30,000	40 @ 2000 Å	GO-9048	Deliyannis
	2290–3110	STIS	1440	30,000	50 @ 3050 Å	GO-7433	Heap
	3030–4515	HIRES	420	49,000	50 @ 3500 Å	H2aH	Boesgaard
	3790–6905	HARPS	60	115,000	100 @ 5000 Å	074.C-0364(A)	Robichon
	5755–8150	HIRES	120	49,000	500 @ 6000 Å	H39aH	Boesgaard
HD 16220	1990–2815	STIS	1975	30,000	30 @ 2100 Å	GO-9048	Deliyannis
	3050–3825	HIRES	100	49,000	150 @ 3500 Å	U11H	Prochaska
	3950–4905	HIRES	100	49,000	300 @ 4500 Å	U11H	Prochaska
	4950–5855	HIRES	100	49,000	200 @ 5500 Å	U11H	Prochaska
HD 76932	1880–2145	STIS	23859	110,000	30 @ 2000 Å	GO-9804	Duncan
	3050–3865	UVES	900	51,000	250 @ 3500 Å	67.D-0439(A)	Primas
	3760–4980	UVES	96	41,000	150 @ 4000 Å	076.B-0055(A)	Silva
	4785–5750	UVES	130	62,000	350 @ 5000 Å	67.D-0439(A)	Primas
	5835–6805	UVES	30	62,000	300 @ 6000 Å	67.D-0439(A)	Primas
HD 94028	1885–2145	STIS	33048	110,000	20 @ 2000 Å	GO-8197	Duncan
	3935–4810[a]	HIRES	270	67,000	200 @ 4500 Å	N01H	Latham
	3695–≈7700	Tull	3300	33,000	145 @ 5200 Å	New observation	Roederer
HD 107113	≈1800–2360	STIS	2281	30,000	40 @ 2000 Å	GO-7433	Heap
	4430–6770	HIRES	180	50,000	350 @ 5000 Å	H2aH	Boesgaard
HD 140283	1935–2210	STIS	8337	110,000	25 @ 2000 Å	GO-7348	Edvardsson
	2390–3135	STIS	11077	50,000	40 @ 3000 Å	GO-9455	Peterson
	3785–6915	HARPS	2700	115,000	250 @ 4500 Å	080.D-0347(A)	Heiter

[a] The iodine cell was inserted during these observations, so we only make use of the blue region of the spectrum unaffected by I_2 absorption.

TABLE 2
Model Atmosphere Parameters and Iron Abundances

Star	$T_{\rm eff}$ (K)	log g	$v_{\rm t}$ (km s^{-1})	[Fe I/H] ± σ	N	[Fe II/H] ± σ	N
HD 2454	6050	4.04	1.20	−0.72 ± 0.10	69	−0.44 ± 0.21	7
HD 16220	6000	3.81	1.30	−0.56 ± 0.14	51	−0.41 ± 0.22	7
HD 76932	5680	4.11	1.00	−1.18 ± 0.12	112	−0.92 ± 0.12	11
HD 94028	5720	4.31	0.90	−1.74 ± 0.09	44	−1.62 ± 0.05	6
HD 107113	6060	3.99	1.25	−0.79 ± 0.08	58	−0.53 ± 0.07	5
HD 140283	5600	3.66	1.15	−2.71 ± 0.05	111	−2.62 ± 0.07	31

Note. — We set the overall metal abundance of the model equal to [Fe II/H].

from Ljung et al. (2006) and Malcheva et al. (2006), as discussed in the Appendix of Roederer et al. (2012); La II from Lawler et al. (2001a); Eu II from Lawler et al. (2001b); and Pb I from Biémont et al. (2000). Hyperfine splitting structure and isotope shifts are considered for As I (Roederer & Lawler 2012), Ba II (McWilliam 1998), La II (Ivans et al. 2006), Eu II (Ivans et al. 2006), and Pb I (Roederer et al. 2012). Uncertainties in the log(gf) values for the elements of interest generally do not contribute significantly to the abundance uncertainties. The Ge I, As I, and Se I transitions used in this study are all major branches (Meggers et al. 1975). Wiese & Martin (1980) estimate accuracies of 25% ($\leq$ 0.10 dex) for the Ge I transition probabilities. The As I and Se I transition probabilities have stated uncertainties of 17% or less ($\leq$ 0.07 dex; see references in Sections 3.3 and 3.4 of Roederer & Lawler 2012). These are relatively small when compared with other sources of uncertainty, but they are included in the random components of uncertainty stated in Tables 4 and 5.

We adopt an r-process isotopic mix (Sneden et al. 2008) for the metal-poor stars and a Solar isotopic mix (Böhlke et al. 2005) for the more metal-rich stars with a relatively large content of s-process material. We do not report abundances for strontium, platinum, or lead in most stars in the sample, unfortunately, because the lines are either undetected or extremely blended. The limited wavelength coverage available for HD 107113 does not cover the strongest lines of Eu II, so we can only derive an upper limit from the non-detection of the intrinsically weak Eu II 6645 Å transition.

We compute uncertainties assuming a minimum measurement (random) uncertainty of 0.10 dex, as estimated from unblended Fe I lines. This accounts for uncertainty in the continuum placement, line fitting, and any mild blending features. Lines marked in Table 3 with ":" indicate we have adopted a minimum measurement uncertainty of 0.20 dex, and lines marked with "::" indicate we have adopted a minimum measurement uncertainty of 0.30 dex. These lines are more blended, and we have had greater difficulty identifying the local continuum. Following Roederer & Lawler (2012), we assume a systematic

TABLE 3
Line-by-Line Abundances

Species	λ (Å)	$\log(gf)$	HD 2454 $\log\epsilon$	HD 16220 $\log\epsilon$	HD 76932 $\log\epsilon$	HD 94028 $\log\epsilon$	HD 107113 $\log\epsilon$	HD 140283 $\log\epsilon$
Zn I	3302.58	−0.02	···	···	+3.56	···	···	···
	4680.14	−0.85	+3.96	+4.13	+3.71	+3.06	+3.88	···
	4722.16	−0.37	+3.91	+4.10	+3.76	+3.10	+3.81	+2.17
	4810.53	−0.15	+4.03	+4.11	+3.79	+3.11	+3.80	+2.09
Zn II	2062.00	−0.29	···	···	···	+3.26	···	+2.27
Ge I	1998.89	−0.78	···	···	···	+1.63:	···	< +1.1
	2041.71	−0.70	···	+3.11::	+2.40	+1.59	+2.54:	< +0.6
	2065.21	−0.79	···	···	···	+1.39:	···	< +0.8
	3039.07	+0.07	+2.70[a]	···	···	···	···	< +0.6
As I	1972.62	−0.63	< +3.9	···	+1.70::	···	+1.87::	+0.09:
	1990.36	−0.28	< +2.9	< +3.1	···	+1.21:	···	···
Se I	1960.89	−0.43	···	···	+2.37::	+2.18:	···	+0.59:
	2039.84	−0.74	···	···	···	+2.03:	···	+0.41
	2074.78	−2.26	< +3.3	+2.83::	+2.45:	+2.03	+2.77:	+0.79
Sr II	4077.71	+0.15	···	···	···	+1.50	···	+0.13
	4215.52	−0.17	···	···	···	+1.52	···	+0.05
Zr II	1996.74	−0.04	···	···	+1.89	+1.36	···	···
	3095.07	−0.84	···	+2.27	+1.84	···	···	···
	3129.76	−0.54	···	···	+1.99	···	···	···
	3273.05	+0.30	+2.69	+2.40	+2.02	···	···	···
	3284.71	−0.37	···	···	+1.97	···	···	···
	3479.39	+0.18	···	···	+1.93	···	···	···
	3505.67	−0.39	···	+2.29	+1.95	···	···	···
	3551.95	−0.36	···	+2.36	+2.00	···	···	···
	3998.96	−0.52	···	···	···	+1.44	···	−0.13
	4050.32	−1.06	+2.64	+2.29	+1.92	+1.46	···	···
	4149.20	−0.04	···	···	···	+1.53	···	−0.22
	4161.20	−0.59	···	···	+1.98	+1.51	···	···
	4208.98	−0.51	+2.68	+2.35	+1.96	+1.48	···	−0.09
	5112.27	−0.85	···	···	···	···	+2.06	···
Ba II	4130.65	+0.52	···	+1.67	+0.95	···	···	···
	4554.03	+0.14	+2.51	+2.23	···	+0.61	+1.94:	−1.37
	5853.68	−0.91	+2.64	+2.07	+1.29	+0.76	+1.79	···
	6141.71	−0.03	···	···	···	···	···	−1.45
	6496.90	−0.41	···	···	···	···	···	−1.29
La II	3988.51	+0.21	+1.05	+0.82	+0.22	−0.24	···	< −1.0
	3995.74	−0.06	+1.06	+0.80	+0.21	−0.34	···	< −1.1
	4086.71	−0.07	+1.23	+0.77	+0.27	−0.28	···	< −1.4
	4123.22	+0.13	+1.11	+0.88	+0.28	−0.25	···	< −1.2
	4662.50	−1.24	···	···	···	···	+0.63	···
	5114.56	−1.03	···	···	···	···	+0.72	···
	6262.29	−1.22	···	···	···	···	+0.67:	···
	6390.48	−1.41	···	···	···	···	+0.62:	···
Eu II	3819.67	+0.51	···	···	···	···	···	< −1.7
	3907.11	+0.17	···	···	−0.11	···	···	< −1.4
	4129.72	+0.22	+0.04	+0.14	−0.17	−0.88	···	< −1.7
	6645.10	+0.12	···	···	−0.11	···	< +0.4	···
Pt I	2049.39	+0.02	···	···	···	+0.20	···	< −0.6
Pb I	4057.81	−0.22	+2.08	···	+1.28	< +1.3	···	< +0.7

[a] Both the STIS and HIRES spectra yield equivalent abundances for this line

uncertainty of 0.19 dex for absorption lines of neutral atoms and 0.29 dex for absorption lines of ions, which accounts for uncertainties in the model atmosphere parameters. The total uncertainty is the quadrature sum of the random and systematic uncertainties, as given in Tables 4 and 5. Most abundance ratios constructed from species in the same ionization state should be fairly robust against uncertainties in the model atmosphere parameters. The combined random uncertainties should adequately represent the uncertainty in these cases, so no total uncertainties are given.

We derive germanium abundances from several lines, including the Ge I 3039 Å line that has been used previously (Sneden et al. 1998, 2003; Cowan et al. 2002, 2005) to study germanium in metal-poor stars. Unfortunately we have not been able to detect both the UV lines near 2000 Å and the 3039 Å line simultaneously, so we cannot verify that these abundance indicators yield consistent results. The subgiants studied in this study and Roederer & Lawler (2012) yield [Ge/Fe] ratios or upper limits that are higher than the samples of giants studied by Cowan et al. (2005) and Roederer et al. (2012). The subgiant sample occupies higher metallicities, so this offset does not necessarily indicate a systematic difference. This issue could be examined with new observations of both sets of Ge I lines in the same star.

Roederer & Lawler (2012) estimated that substantial fractions (≈ 10%–90%) of neutral arsenic and selenium are present in the line-forming layers of the atmosphere of HD 160617. Both elements have relatively high first ionization potentials (FIPs), 9.79 eV and 9.75 eV, respectively. Germanium has a somewhat lower FIP, 7.90 eV.

TABLE 4
Mean Abundances for HD 2454, HD 16220, and HD 76932

Element or Ratio	HD 2454				HD 16220				HD 76932			
	value	$\sigma_{\rm random}$	$\sigma_{\rm total}$	N	value	$\sigma_{\rm random}$	$\sigma_{\rm total}$	$N_{\rm lines}$	value	$\sigma_{\rm random}$	$\sigma_{\rm total}$	N
$\log\epsilon$ (Fe I)	+6.78	0.10	0.21	69	+6.94	0.14	0.24	51	+6.32	0.12	0.22	112
$\log\epsilon$ (Fe II)	+7.06	0.21	0.36	7	+7.09	0.22	0.36	7	+6.58	0.12	0.31	11
$\log\epsilon$ (Zn I)	+3.97	0.07	0.20	3	+4.11	0.06	0.20	3	+3.71	0.06	0.20	4
$\log\epsilon$ (Zn II)	···	···	···	0	···	···	···	0	···	···	···	0
$\log\epsilon$ (Ge I)	+2.70	0.14	0.24	1	+3.11	0.32	0.37	1	+2.40	0.14	0.24	1
$\log\epsilon$ (As I)	< +2.9	···	···	2	< +3.1	···	···	1	+1.70	0.31	0.36	1
$\log\epsilon$ (Se I)	< +3.3	···	···	1	+2.83	0.30	0.36	1	+2.41	0.16	0.25	2
$\log\epsilon$ (Sr II)	···	···	···	0	···	···	···	0	···	···	···	0
$\log\epsilon$ (Zr II)	+2.66	0.06	0.30	3	+2.33	0.05	0.29	6	+1.95	0.06	0.30	11
$\log\epsilon$ (Ba II)	+2.58	0.12	0.31	2	+1.99	0.33	0.44	3	+1.12	0.31	0.42	2
$\log\epsilon$ (La II)	+1.11	0.09	0.30	4	+0.82	0.06	0.30	4	+0.24	0.09	0.30	4
$\log\epsilon$ (Eu II)	+0.04	0.10	0.31	1	+0.14	0.10	0.31	1	−0.13	0.07	0.30	3
$\log\epsilon$ (Pt I)	···	···	···	0	···	···	···	0	···	···	···	0
$\log\epsilon$ (Pb I)	+2.08	0.10	0.21	1	···	···	···	0	+1.28	0.10	0.21	1
[Fe I/H]	−0.72	0.10	···	69	−0.56	0.14	···	51	−1.18	0.12	···	112
[Fe II/H]	−0.44	0.21	···	7	−0.41	0.22	···	7	−0.92	0.12	···	11
[Zn I/Fe I]	+0.13	0.12	···	3	+0.11	0.15	···	3	+0.33	0.13	···	4
[Zn II/Fe II]	···	···	···	0	···	···	···	0	···	···	···	0
[Ge I/Fe I]	−0.23	0.17	···	1	+0.02	0.35	···	1	−0.07	0.19	···	1
[As I/Fe I]	< +1.32	···	···	2	< +1.36	···	···	1	+0.58	0.33	···	1
[Se I/Fe I]	< +0.68	···	···	1	+0.05	0.33	···	1	+0.25	0.20	···	2
[Sr II/Fe II]	···	···	···	0	···	···	···	0	···	···	···	0
[Zr II/Fe II]	+0.52	0.22	···	3	+0.16	0.23	···	6	+0.29	0.13	···	11
[Ba II/Fe II]	+0.84	0.24	···	2	+0.22	0.40	···	3	−0.14	0.33	···	2
[La II/Fe II]	+0.45	0.23	···	4	+0.13	0.23	···	4	+0.06	0.15	···	4
[Eu II/Fe II]	−0.04	0.23	···	1	+0.03	0.24	···	1	+0.27	0.14	···	3
[Pt I/Fe I]	···	···	···	0	···	···	···	0	···	···	···	0
[Pb I/Fe I]	+0.76	0.14	···	1	···	···	···	0	+0.42	0.16	···	1

TABLE 5
Mean Abundances for HD 94028, HD 107113, and HD 140283

Element or Ratio	HD 94028				HD 107113				HD 140283			
	value	$\sigma_{\rm random}$	$\sigma_{\rm total}$	N	value	$\sigma_{\rm random}$	$\sigma_{\rm total}$	$N_{\rm lines}$	value	$\sigma_{\rm random}$	$\sigma_{\rm total}$	N
$\log\epsilon$ (Fe I)	+5.75	0.09	0.21	44	+6.71	0.08	0.21	58	+4.79	0.05	0.20	109
$\log\epsilon$ (Fe II)	+5.88	0.05	0.29	6	+6.97	0.07	0.30	5	+4.88	0.06	0.30	28
$\log\epsilon$ (Zn I)	+3.09	0.06	0.20	3	+3.83	0.06	0.20	3	+2.13	0.07	0.20	2
$\log\epsilon$ (Zn II)	+3.26	0.10	0.31	1	···	···	···	0	+2.27	0.10	0.31	1
$\log\epsilon$ (Ge I)	+1.56	0.17	0.26	3	+2.54	0.22	0.29	1	< +0.6	···	···	4
$\log\epsilon$ (As I)	+1.21	0.21	0.28	1	+1.87	0.31	0.36	1	+0.09	0.21	0.28	1
$\log\epsilon$ (Se I)	+2.06	0.17	0.25	3	+2.77	0.21	0.28	1	+0.60	0.24	0.31	3
$\log\epsilon$ (Sr II)	+1.51	0.07	0.30	2	···	···	···	0	+0.09	0.07	0.30	2
$\log\epsilon$ (Zr II)	+1.46	0.07	0.30	6	+2.06	0.10	0.31	1	−0.15	0.08	0.30	3
$\log\epsilon$ (Ba II)	+0.68	0.13	0.32	2	+1.82	0.14	0.32	2	−1.37	0.10	0.31	3
$\log\epsilon$ (La II)	−0.28	0.05	0.29	4	+0.67	0.05	0.29	4	< −1.4	···	···	4
$\log\epsilon$ (Eu II)	−0.88	0.10	0.31	1	< +0.4	···	···	1	< −1.7	···	···	3
$\log\epsilon$ (Pt I)	+0.20	0.10	0.21	1	···	···	···	0	< −0.6	···	···	1
$\log\epsilon$ (Pb I)	< +1.3	···	···	1	···	···	···	0	< +0.7	···	···	1
[Fe I/H]	−1.75	0.09	···	44	−0.79	0.08	···	58	−2.71	0.05	···	109
[Fe II/H]	−1.62	0.05	···	6	−0.53	0.07	···	5	−2.62	0.06	···	28
[Zn I/Fe I]	+0.28	0.11	···	3	+0.06	0.10	···	3	+0.28	0.09	···	2
[Zn II/Fe II]	+0.32	0.11	···	1	···	···	···	0	+0.33	0.12	···	1
[Ge I/Fe I]	−0.34	0.19	···	3	−0.32	0.24	···	1	< −0.34	···	···	4
[As I/Fe I]	+0.66	0.23	···	1	+0.36	0.32	···	1	+0.50	0.22	···	1
[Se I/Fe I]	+0.47	0.19	···	3	+0.22	0.23	···	1	−0.03	0.25	···	3
[Sr II/Fe II]	+0.26	0.09	···	2	···	···	···	0	−0.16	0.09	···	2
[Zr II/Fe II]	+0.50	0.09	···	6	+0.01	0.12	···	1	−0.11	0.10	···	3
[Ba II/Fe II]	+0.12	0.14	···	2	+0.17	0.16	···	2	−0.93	0.12	···	3
[La II/Fe II]	+0.24	0.07	···	4	+0.10	0.09	···	4	< +0.12	···	···	4
[Eu II/Fe II]	+0.22	0.11	···	1	< +0.41	···	···	1	< +0.40	···	···	3
[Pt I/Fe I]	+0.33	0.13	···	1	···	···	···	0	< +0.49	···	···	1
[Pb I/Fe I]	< +1.01	···	···	1	···	···	···	0	< +1.37	···	···	1

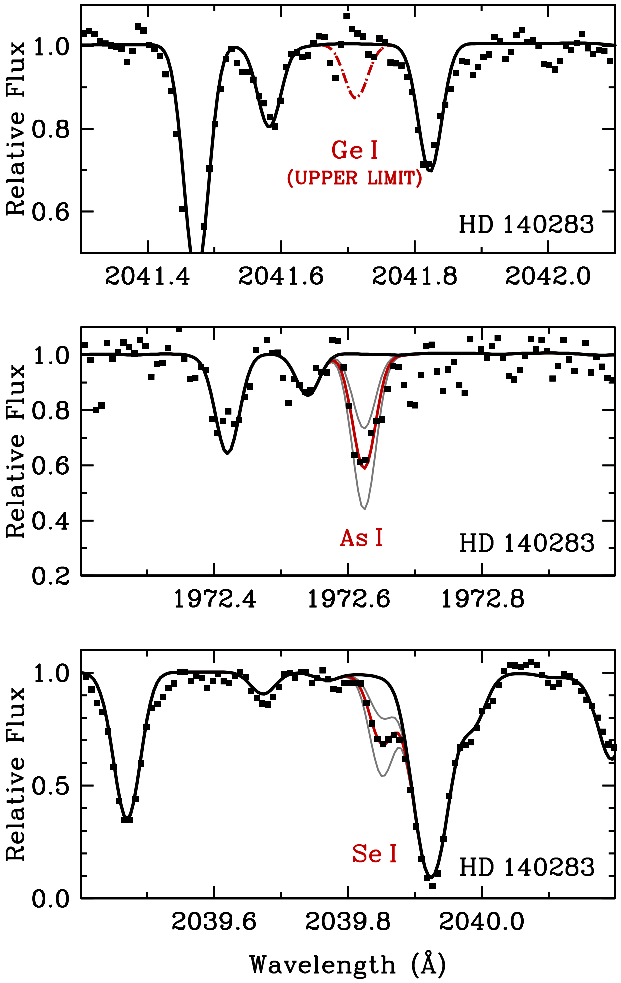

Fig. 1.— Synthesis of a sample of Ge i, As i, and Se i lines in the UV STIS spectrum of HD 140283. In the top panel, the Ge i upper limit (3σ) is indicated by the dot-dashed line. In the lower two panels, the best-fit synthesis is indicated by the bold red line. The light gray lines show variations in the best-fit abundance by ± 0.3 dex. In all three panels, the bold black line indicates a synthesis with no Ge i, As i, or Se i present.

Our calculations reveal that ≈ 3%–9% of the germanium in the line-forming layers is neutral; while small, this is a substantially higher percentage of Ge i than, e.g., Fe i expected in the line-forming layers of these warm subgiants. The lower levels of the Ge i transitions used in our study comprise the main population reservoirs ($>$ 98%) for Ge i at the temperatures found in these atmospheres, although the fraction of all germanium atoms in a given level never exceeds 1%–2%. Our calculations assume that the level populations and ionization fractions can be described by Boltzmann and Saha distributions in local thermodynamical equilibrium (LTE). We caution that our LTE calculations may underestimate the total germanium abundance due to the minority species Ge i being driven out of LTE by overionization. Estimating the possible magnitude of this effect is beyond the scope of the present study, although we would expect the non-LTE corrections to be similar for all stars in our sample. Non-LTE calculations of the germanium line formation in these stars would be most welcome.

Mashonkina et al. (2012) have estimated non-LTE corrections to the abundances derived from the Pb i 4057 Å and Eu ii 4129 Å lines in the sample of stars examined by Roederer et al. (2010). Neutral lead atoms are no more than a couple percent of the total fraction of lead in metal-poor subgiants or turnoff stars, so the corrections may be substantial. Mashonkina et al. calculate non-LTE corrections of approximately +0.25 to +0.40 dex for the Pb i 4057 Å line in stars like those in our sample. Their calculated non-LTE corrections for the Eu ii 4129 Å line are small, typically +0.05 dex. We do not include these corrections to the values presented in Tables 4 and 5, but we caution that the lead abundances listed may be underestimated by a factor of 2 or so.

For optical wavelengths of interest to abundance studies of late-type stars, the continuous opacity is dominated by bound-free (bf) absorption of the H^- ion. Rayleigh scattering and bf absorption from atomic H also contribute to a lesser degree. At UV wavelengths in stars of high metallicity, bf absorption from neutral metals also becomes a significant source of continuous opacity. Our calculations indicate that the opacity is dominated by $H^-_{\rm bf}$ absorption in these stars at most wavelengths of interest to the present study. H $\textsc{i}_{\rm bf}$ also contributes significantly at wavelengths short of the Balmer jump. Bf absorption from the Mg i $3s3p\ ^3P^o$ term and the Al i $3s^23p\ ^2P^o$ term occurs short of 2515 Å and 2076 Å, respectively. The contributions to the total continuous opacity from these metals are comparable to—but do not dominate—the contributions from H only in the most metal-rich stars ([Fe/H] ≈ −0.5) in our sample. In these stars, abundance ratios derived from lines in our UV spectra near 2000 Å could be referenced to either H or Al, since these elements both contribute roughly equally to the total continuous opacity. In the more metal-poor stars, H still dominates the sources of continuous opacity near 2000 Å. We underscore the fact that most of the lines of interest of Ge i, As i, and Se i occur within a narrow wavelength range, so abundance ratios among these elements should be quite robust.

Our derived mean abundances are listed in Tables 4 and 5. Both log ϵ abundances and [X/Fe] ratios are given. Recall that abundances or ratios denoted with the ionization state represent the total abundance of that element as derived from absorption lines of the species indicated. Note that the [Zn/Fe] ratios derived from both neutral and ionized zinc are in agreement in HD 94028 and HD 140283, as Roederer & Lawler (2012) also found for HD 160617.

5. RESULTS AND DISCUSSION

5.1. *The Nature of Our Sample*

The stars in our sample span a wide range of ages, metallicities, and Galactic stellar populations. The three most metal-rich stars in our sample, HD 2454, HD 16220, and HD 107113, have overall metallicities [Fe/H] ≈ −0.5. These stars have kinematics consistent with membership in the thin disc, are approximately 2–4 Gyr old, and have only mildly enhanced [α/Fe] ratios (where α stands for O, Mg, Si, Ca, or Ti), $+0.05 \leq [\alpha/\mathrm{Fe}] \leq +0.15$ (e.g., Edvardsson et al. 1993; Venn et al. 2004; Bensby et al. 2005; Holmberg et al. 2009; Casagrande et al. 2011). HD 76932 is more

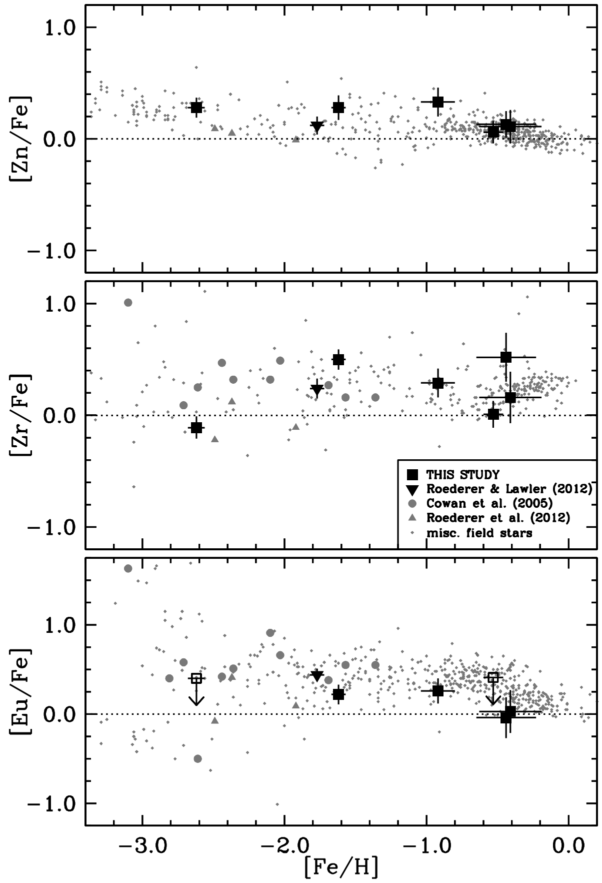

FIG. 2.— The [Zn/Fe], [Zr/Fe], and [Eu/Fe] ratios as a function of [Fe/H]. Stars examined in this study are marked by the large black squares. The other star where germanium, arsenic, and selenium have been studied, HD 160617, is marked by the large black triangle. Other stars where germanium has been studied are marked by medium-sized gray circles (Cowan et al. 2005) or medium-sized gray triangles (Roederer et al. 2012). These studies included several stars that had been examined previously by Sneden et al. (1998, 2003) and Cowan et al. (2002). Filled symbols denote detections, and open symbols denote upper limits. Abundances of field stars derived by various surveys are taken from Burris et al. (2000), Fulbright (2000), Reddy et al. (2003, 2006), Cayrel et al. (2004), François et al. (2007), and Roederer et al. (2010). The dotted horizontal lines indicate the Solar ratios.

metal poor, [Fe/H] = −0.9, is a probable member of the thick disc, has an intermediate age of approximately 7–11 Gyr, and has significant α-enhancement, [α/Fe] = +0.3 (e.g., Edvardsson et al. 1993; Venn et al. 2004; Nissen & Schuster 2010; Casagrande et al. 2011; Schuster et al. 2012). The three most metal-poor stars, HD 94028, HD 140283, and HD 160617, have metallicities spanning $-2.6 \leq$ [Fe/H] ≤ -1.6. These stars have kinematics consistent with the thick disc or halo, have ages of 12 Gyr or more, and have enhanced [α/Fe] ratios, $+0.3 \leq$ [α/Fe] $\leq +0.4$ (e.g., Fulbright 2000; Venn et al. 2004; Holmberg et al. 2009; Casagrande et al. 2011; Roederer & Lawler 2012).

In Figure 2, we compare the [Zn/Fe], [Zr/Fe], and [Eu/Fe] ratios for the stars in our sample (black squares and triangle) with previous surveys of the Galactic halo, thick, and thin discs (small diamonds). We also highlight stars with previous [Ge/Fe] determinations (gray circles and triangles). When necessary, we correct the log(gf) scales to those used in the present study.[2] The two most metal-rich stars in our sample have [Eu/Fe] ratios consistent with the Solar ratio, which is on the low end of the field star distribution near [Fe/H] = −0.4. One of them, HD 2454, is a known barium dwarf star and will be discussed separately in Section 5.3. Overall these stars fall well within the ranges of [Zn/Fe], [Zr/Fe], and [Eu/Fe] for field stars at similar metallicity. This demonstrates that the stars of interest for the present study are not outliers according to their chemistry.

5.2. *Germanium Trends with Metallicity*

Figures 3 and 4 indicate that the [Ge/Fe] and [Ge/Zn] ratios increase with increasing metallicity. The increase in [Ge/Fe] begins at least by [Fe/H] = −1.6, and the four stars in our sample with [Fe/H] > −1.0 show [Ge/Fe] ratios close to the Solar ratio. Other stars with [Fe/H] = −1.6 show low [Ge/Fe] ratios that are consistent with those found in the class of r-process rich standard stars, whose members include BD+17 3248 (Cowan et al. 2002), CS 22892–052 (Sneden et al. 2003), CS 31082–001 (Hill et al. 2002), HD 115444 (Westin et al. 2000), and HD 221170 (Ivans et al. 2006). Previous observations of metal-poor stars show that [Ge/Fe] does not correlate with [Eu/Fe], a common tracer of the main component of the r-process, indicating that germanium is not produced under the same conditions that give rise to r-process nucleosynthesis. This result was initially found by Cowan et al. (2005), and more recent observations reaffirm it (Roederer et al. 2012).

The overall increase and scatter in [Ge/Fe] echoes the increase and scatter in [La/Eu] found in many field stars over the same metallicity range, as shown in Figure 5. The lowest metallicity stars and some even at metallicity [Fe/H] = −1.4 show a low [La/Eu] ratio that is consistent with the [La/Eu] ratio found in the r-process rich standard stars (shaded band in Figure 5). A range of [La/Eu] ratios is found at most metallicities, but the upturn in [La/Eu] toward the Solar ratio with increasing metallicity generally is attributed to increasing amounts of s-process material present in the ISM when these stars were born (e.g., Simmerer et al. 2004). It is reasonable to conclude that the increase in [Ge/Fe] ratios may also be due to increasing amounts of s-process material present in the ISM. We dedicate the next sections to investigating the nature of the s-process that could be responsible for the germanium production.

5.3. *The Barium Star HD 2454*

---

[2] Large surveys concerned with the chemical evolution of the thin disc find that the mean [Zr/Fe] ratio converges to the Solar ratio at Solar metallicity (e.g., Edvardsson et al. 1993; Reddy et al. 2003). In our Figure 2, however, the Zr II abundances for stars near Solar metallicity, mostly derived by Reddy et al., appear to converge toward [Zr/Fe] = +0.3 at [Fe/H] = 0.0. Reddy et al. used one Zr II line, 5112 Å, and they adopted its log(gf) value from Biémont et al. (1981) and Bogdanovich et al. (1996), which is 0.26 dex higher than the value presented by Ljung et al. (2006). The discrepancy stems from the smaller experimental branching fraction measured by Ljung et al. relative to the values available previously. The log(gf) value given by Ljung et al. yields a Zr II abundance derived from the the 5112 Å line in the Solar photosphere that is in better agreement with other lines, and we prefer this value.

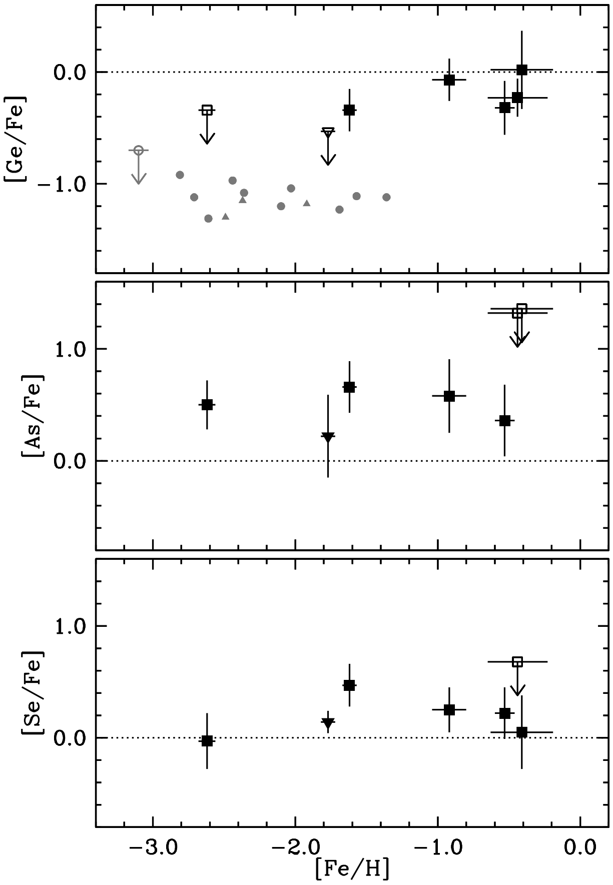

Fig. 3.— The [Ge/Fe], [As/Fe], and [Se/Fe] ratios as a function of [Fe/H]. Symbols are the same as in Figure 2. Filled symbols denote detections, and open symbols denote upper limits.

Tomkin et al. (1989) identified HD 2454 (HR 107), which is in our sample, as the first example of a barium dwarf star. Such stars may be the dwarf analogs of the classical barium giants, Population I stars in binary systems with strong lines of Ba II, Sr II, C_2, CH, and CN. These stars may be formed by accreting mass from a more massive companion that passed through the AGB phase of evolution.

A recent study of the heavy element abundance pattern in HD 2454 by Allen & Barbuy (2006) reveals substantial overabundances of elements at all three *s*-process peaks, as well as a mild carbon overabundance, supporting this interpretation. The *s*-process pattern in this star (either their abundances or ours) can be reasonably fit by the *s*-process abundance predictions of Husti et al. (2009) and Bisterzo et al. (2010) for an AGB star with an initial main sequence mass of $1.2 \lesssim M/M_{\odot} \lesssim 3.0$, metallicity [Fe/H] ≈ -0.5, and a fairly standard ^{13}C pocket efficiency. All but the stars of lowest mass in this range will evolve in less than ≈ 2 Gyr, which is less than the inferred age of the observed main sequence star, ≈ 2.0–2.5 Gyr (Bensby et al. 2005; Casagrande et al. 2011).

We find that the [Zr/Fe], [Ba/Fe], and [La/Fe] ratios in HD 2454 are enhanced by factors of 2–4 relative to these ratios in HD 16220, which has a nearly identical metallicity and [Eu/Fe] ratio as HD 2454. (The [Pb/Fe] ratio in HD 2454 is also enhanced; we could not derive [Pb/Fe] in HD 16220.) The [Ge/Fe] ratios are identical within the uncertainties in HD 2454 and HD 16220, however, suggesting that the nucleosynthesis process responsible for the enhancements at the three *s*-process peaks in the AGB companion did not produce any detectable germanium. In this scenario, the germanium enrichment was present in the birth cloud of HD 2454, while most of the enrichment of zirconium, barium, and lanthanum occurred via mass transfer from a binary companion that passed through the AGB phase.

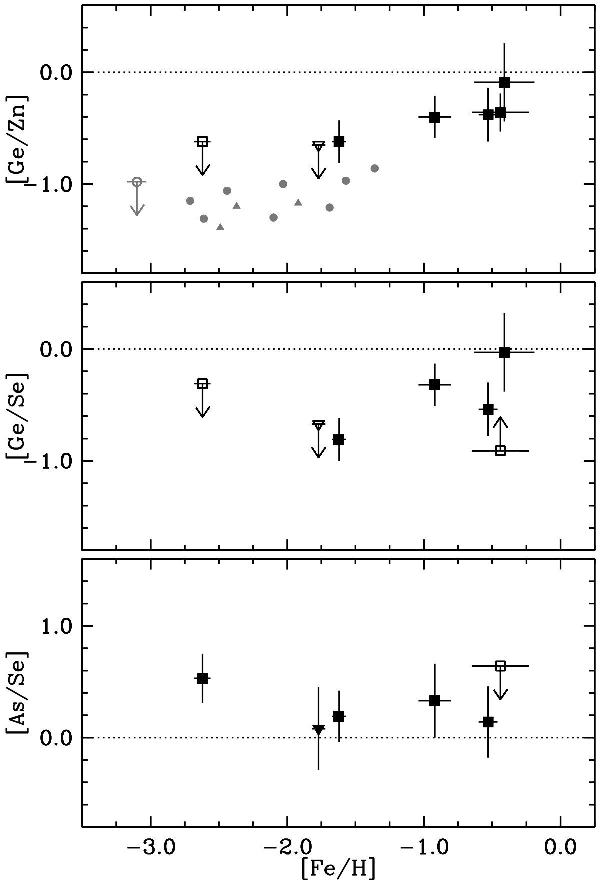

Fig. 4.— The [Ge/Zn], [Ge/Se], and [As/Se] ratios as a function of [Fe/H]. Symbols are the same as in Figure 2. Filled symbols denote detections, and open symbols denote limits. The upward arrow in the middle panel denotes a lower limit on [Ge/Se] from an upper limit on the selenium abundance.

5.4. *Nucleosynthesis of Germanium*

Our data indicate that the nucleosynthesis process responsible for the increasing [Ge/Fe] ratios should produce substantial germanium, relatively small amounts of zinc, arsenic, and selenium (see Section 5.6), and little material with $A \gtrsim 90$. If we attribute the enrichment of elements at the *s*-process peaks in HD 2454 to the main component of the *s*-process, then the overall upturn in [Ge/Fe] could be the result of the weak component of the *s*-process. This is consistent with longstanding interpretations of the origin of the A $\lesssim$ 90 portion of the Solar system *s*-process distribution (e.g., Käppeler et al. 1989; Raiteri et al. 1991), where 80% of the germanium is estimated to have originated in the weak component of the *s*-process operating in massive ($M \sim 25\ M_{\odot}$) stars (e.g., Pignatari et al. 2010).

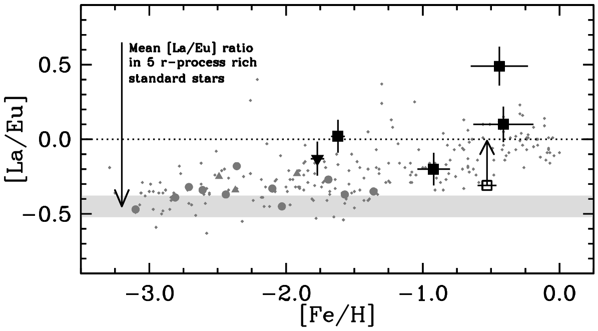

FIG. 5.— The [La/Eu] ratio as a function of [Fe/H]. Symbols are the same as in Figure 2. Filled symbols denote detections, and open symbols denote limits. The upward arrow denotes a lower limit on [La/Eu] from an upper limit on the europium abundance. The gray shaded band represents the mean [La/Eu] ratio found in 5 *r*-process rich standard stars, as analyzed by Sneden et al. (2009), $\langle[\mathrm{La/Eu}]\rangle = -0.45 \pm 0.07$. The field sample includes additional stars from Simmerer et al. (2004) and their reanalysis of stars examined by Woolf et al. (1995).

The germanium in the more metal-poor stars seems to have been produced by a different mechanism. The germanium in these stars may have been produced by previous stellar generations under conditions of nuclear statistical equilibrium (e.g., Wanajo et al. 2011) or charged-particle reactions (e.g., Fröhlich et al. 2006). Perhaps the ISM in the birth environments of most metal-poor stars was not widely enriched by products of the weak *s*-process. Alternatively, the *s*-process that was in operation in massive, low-metallicity stars may have been fundamentally different than that in metal-rich stars.

5.5. *Arsenic and Selenium Trends with Metallicity*

Figures 3 and 4 show the evolution of the [As/Fe], [Se/Fe], and [As/Se] ratios as a function of metallicity. Although there are only 7 stars available at present to trace the evolution of these elements, a few points can be inferred from these figures. There appears to be relatively little evolution in either the [As/Fe] or [Se/Fe] ratios from $-2.6 < [\mathrm{Fe/H}] < -0.4$. The mean [As/Fe] ratio is $+0.51 \pm 0.08$ ($\sigma = 0.18$), and the mean [Se/Fe] ratio is $+0.19 \pm 0.07$ ($\sigma = 0.18$). Unsurprisingly, the [As/Se] trend is also relatively flat. In contrast, the [Ge/Se] ratio suggests an upward trend with increasing metallicity. At low metallicity, $[\mathrm{Fe/H}] < -0.9$, the [As/Fe] ratios are enhanced similarly to [Eu/Fe]. [Se/Fe] is less enhanced but still super-Solar, except possibly in HD 140283. Our metal-poor sample does not include any stars with extreme values of [Eu/Fe], so we cannot investigate trends between arsenic or selenium and europium as Cowan et al. (2005) did for germanium. We could only derive upper limits on arsenic and selenium in HD 2454, the barium dwarf star, since the lines are too blended to be reliable abundance indicators.

5.6. *Nucleosynthesis of Arsenic and Selenium*

Our observations indicate [Ge/Se] is trending toward the Solar ratio at high metallicity, while [As/Se] remains Solar or super-Solar. Neither [As/Fe] nor [Se/Fe] appear to be affected by the weak *s*-process in the way that [Ge/Fe] is. This result is consistent with the relatively small fraction of arsenic and selenium in the Solar system attributed to the *s*-process. The rapidly-rotating massive star models of Frischknecht et al. (2012) predict that *s*-process production of germanium should be accompanied by production of arsenic and selenium by similar factors. While the weak *s*-process may contribute small amounts of arsenic and selenium that are undetected amidst a relatively large primary abundance, our data exclude it as a major source of the arsenic and selenium in the metal-rich stars.

HD 16220, HD 76932, HD 94028, HD 107113, and HD 160617 all have [La/Eu] ratios enhanced significantly above the mean [La/Eu] found in the *r*-process standard stars, as shown in Figure 5. This indicates that material produced by the main component of the *s*-process was incorporated into these stars. The intermediate mass AGB models of Karakas et al. (2009) that cover a range of metallicities predict approximately Solar [Ge/Se] ratios, and the low mass models predict $[\mathrm{Ge/Se}] \approx -0.15$ to -0.20. This is also the case at very low metallicity; see the models in Lugaro et al. (2012). These models also predict that [As/Se] should be sub-Solar by a factor of ≈ 2 (A. Karakas, 2012, private communication). The relatively constant and super-Solar [As/Fe], [Se/Fe], and [As/Se] ratios indicate that the main component of the *s*-process also contributed little to these elements in our stellar sample.

Simulations of *r*-process nucleosynthesis predict that conditions leading to the production of these elements should be different than the conditions leading to the main component of the *r*-process (e.g., Kratz et al. 2007; Farouqi et al. 2009). As with germanium in low metallicity stars, explosive nucleosynthesis in nuclear statistical equilibrium (e.g., Wanajo et al. 2011) or a charged-particle process (e.g., Fröhlich et al. 2006) are likely candidates, but these data cannot affirm this specifically. Detection of arsenic and selenium in stars with $[\mathrm{Fe/H}] < -2.0$ and low [Ge/Fe] and [La/Eu] ratios would help diagnose this matter.

6. CONCLUSIONS

We present a study of the chemical evolution of germanium, arsenic, and selenium in metal-poor stars. Of these three elements, only germanium abundances have been studied previously in multiple metal-poor stars, and that only for stars with $[\mathrm{Fe/H}] \leq -1.4$ (Sneden et al. 1998, 2003; Cowan et al. 2002, 2005; Roederer et al. 2012). Using archive space-based UV spectra obtained with STIS on board the *HST* and ground-based optical spectra from several observatories, we are able to study abundances of these elements in seven stars spanning metallicities $-2.6 \leq [\mathrm{Fe/H}] \leq -0.4$. We also derive abundances of zinc, strontium, zirconium, barium, lanthanum, europium, platinum, and lead to inform our interpretation.

The stars in our sample appear to be normal chemical representatives of the halo, thick, and thin discs. Previous observations indicate that germanium tracks iron at low metallicity (Cowan et al. 2005). Our new observations indicate that [Ge/Fe] ratios increase at higher metallicities, presumably due to production by the weak component of the *s*-process. [As/Fe] and [Se/Fe] show no such increase, suggesting that their dominant production mechanism may be the same at both low and high metallicity. Explosive nucleosynthesis or charged-particle reactions are likely mechanisms for arsenic and selenium production, though our data are agnostic about this point. Our data imply that the main component of the *s*-process has contributed very little to the germanium, arsenic, or selenium in our stellar sample.

These results are not in conflict with theoretical predictions for the origin of germanium, arsenic, and selenium in the Solar system. Considering the scarce abundance data on these elements available beyond the Solar abundance distribution, we find this agreement encouraging.

Finally, we underscore that our conclusions have been drawn from abundances in a very small number of stars. Studies of arsenic and selenium in metal-poor stars are reliant on access to high resolution, high S/N UV spectra attainable only with *HST*. This has been, and will remain, the limiting factor in such studies for the foreseeable future.

I am especially grateful to the many observers whose data have made this study possible. I thank A. Karakas and M. Pignatari for helpful conversations on *s*-process nucleosynthesis and the referee, Charles Cowley, for a careful reading of the manuscript. This research has made use of NASA's Astrophysics Data System Bibliographic Services, the arXiv pre-print server operated by Cornell University, the SIMBAD and VizieR databases hosted by the Strasbourg Astronomical Data Center, the Atomic Spectra Database hosted by the National Institute of Standards and Technology, the Mikulski Archive at the Space Telescope Science Institute, the ESO Science Archive Facility, and the Keck Observatory Archive. IRAF is distributed by the National Optical Astronomy Observatories, which are operated by the Association of Universities for Research in Astronomy (AURA), Inc., under cooperative agreement with the National Science Foundation. This research is supported in part by NASA through a grant to Program GO-12268 from the Space Telescope Science Institute, which is operated by AURA under NASA contract NAS 5-26555. I.U.R. is supported by the Carnegie Institution of Washington through the Carnegie Observatories Fellowship.

Facilities: ESO:3.6m (HARPS), HST (STIS), Keck:I (HIRES), Smith (Tull), VLT:Kueyen (UVES)

REFERENCES

Allen, D. M., & Barbuy, B. 2006, A&A, 454, 895
Alonso, A., Arribas, S., & Martínez-Roger, C. 1999, A&AS, 139, 335
Arlandini, C., Käppeler, F., Wisshak, K., et al. 1999, ApJ, 525, 886
Asplund, M., Grevesse, N., Sauval, A. J., & Scott, P. 2009, ARA&A, 47, 481
Ayres, T. R. 2010, ApJS, 187, 149
Barklem, P. S., Piskunov, N., & O'Mara, B. J. 2000, A&AS, 142, 467
Barklem, P. S., & Aspelund-Johansson, J. 2005, A&A, 435, 373
Bensby, T., Feltzing, S., Lundström, I., & Ilyin, I. 2005, A&A, 433, 185
Bidelman, W. P., & Corliss, C. H. 1962, ApJ, 135, 968
Biémont, E., Grevesse, N., Hannaford, P., & Lowe, R. M. 1981, ApJ, 248, 867
Biémont, E., Garnir, H. P., Palmeri, P., Li, Z. S., & Svanberg, S. 2000, MNRAS, 312, 116
Bisterzo, S., Gallino, R., Straniero, O., Cristallo, S., Käppeler, F. 2010, MNRAS, 404, 1529
Bisterzo, S., Gallino, R., Straniero, O., Cristallo, S., Käppeler, F. 2011, MNRAS, 418, 284
Bogdanovich, P., Tautvaisiene, G., Rudzikas, Z., & Momkauskaite, A. 1996, MNRAS, 280, 95
Böhlke, J. K., de Laeter, J. R., De Bièvre, P., et al. 2005, Journal of Physical and Chemical Reference Data, 34, 57
Burris, D. L., Pilachowski, C. A., Armandroff, T. E., et al. 2000, ApJ, 544, 302
Cameron, A. G. W. 1982, Ap&SS, 82, 123
Cardelli, J. A., Savage, B. D., & Ebbets, D. C. 1991, ApJ, 383, L23
Casagrande, L., Schönrich, R., Asplund, M., et al. 2011, A&A, 530, A138
Castelli, F., & Kurucz, R. L. Proc. IAU Symp. No 210, Modelling of Stellar Atmospheres, N. Piskunov et al., eds. 2003, A20
Castelli, F., & Hubrig, S. 2004, A&A, 425, 263
Cayrel, R., Depagne, E., Spite, M., et al. 2004, A&A, 416, 1117
Cowan, J. J., Sneden, C., Burles, S., et al. 2002, ApJ, 572, 861
Cowan, J. J., Sneden, C., Beers, T. C., et al. 2005, ApJ, 627, 238
Cowley, C. R., Hubrig, S., & González, J. F. 2010, A&A, 523, A82
Dekker, H., D'Odorico, S., Kaufer, A., Delabre, B., & Kotzlowski, H. 2000, Proc. SPIE, 4008, 534
Dinerstein, H. L. 2001, ApJ, 550, L223
Edvardsson, B., Andersen, J., Gustafsson, B., et al. 1993, A&A, 275, 101
Farouqi, K., Kratz, K.-L., Mashonkina, L. I., et al. 2009, ApJ, 694, L49
François, P., Depagne, E., Hill, V., et al. 2007, A&A, 476, 935
Frischknecht, U., Hirschi, R., & Thielemann, F.-K. 2012, A&A, 538, L2
Fröhlich, C., Martínez-Pinedo, G., Liebendörfer, M., et al. 2006, Physical Review Letters, 96, 142502
Fuhr, J. R., & Wiese, W. L. 2006, Journal of Physical and Chemical Reference Data, 35, 1669
Fuhr, J. R. & Wiese, W. L. 2009, Atomic Transition Probabilities, published in the CRC Handbook of Chemistry and Physics, 90th Edition, Lide, D. R., ed. CRC Press, Inc., Boca Raton, FL, 10
Fulbright, J. P. 2000, AJ, 120, 1841
Gallino, R., Arlandini, C., Busso, M., et al. 1998, ApJ, 497, 388
Hill, V., Plez, B., Cayrel, R., et al. 2002, A&A, 387, 560
Hobbs, L. M., Welty, D. E., Morton, D. C., Spitzer, L., & York, D. G. 1993, ApJ, 411, 750
Holmberg, J., Nordström, B., & Andersen, J. 2009, A&A, 501, 941
Husti, L., Gallino, R., Bisterzo, S., Straniero, O., & Cristallo, S. 2009, Publ. Astr. Soc. Australia, 26, 176
Ivans, I. I., Sneden, C., James, C. R., et al. 2003, ApJ, 592, 906
Ivans, I. I., Simmerer, J., Sneden, C., et al. 2006, ApJ, 645, 613
Käppeler, F., Beer, H., Wisshak, K., et al. 1982, ApJ, 257, 821
Käppeler, F., Beer, H., & Wisshak, K. 1989, Reports on Progress in Physics, 52, 945
Karakas, A. I., Lugaro, M., & Gallino, R. 2007, ApJ, 656, L73
Karakas, A. I., van Raai, M. A., Lugaro, M., Sterling, N. C., & Dinerstein, H. L. 2009, ApJ, 690, 1130
Kimble, R. A., Woodgate, B. E., Bowers, C. W., et al. 1998, ApJ, 492, L83
Klose, J. Z., Fuhr, J. R., & Wiese, W. L. 2002, Journal of Physical and Chemical Reference Data, 31, 217
Kratz, K.-L., Farouqi, K., Pfeiffer, B., et al. 2007, ApJ, 662, 39
Kurucz, R. L., & Bell, B. 1995, Kurucz CD-ROM, Cambridge, MA: Smithsonian Astrophysical Observatory
Lawler, J. E., Bonvallet, G., & Sneden, C. 2001a, ApJ, 556, 452
Lawler, J. E., Wickliffe, M. E., Den Hartog, E. A., & Sneden, C. 2001b, ApJ, 563, 1075
Leckrone, D. S., Proffitt, C. R., Wahlgren, G. M., Johansson, S. G., & Brage, T. 1999, AJ, 117, 1454
Ljung, G., Nilsson, H., Asplund, M., & Johansson, S. 2006, A&A, 456, 1181
Lugaro, M., Karakas, A. I., Stancliffe, R. J., & Rijs, C. 2012, ApJ, 747, 2
Malcheva, G., Blagoev, K., Mayo, R., et al. 2006, MNRAS, 367, 754
Mashonkina, L., Ryabtsev, A., & Frebel, A. 2012, A&A, 540, A98
Mayor, M., Pepe, F., Queloz, D., et al. 2003, The Messenger, 114, 20
McWilliam, A. 1998, AJ, 115, 1640

Meggers, W. F., Corlis, C. H., & Scribner, B. F. 1975, Tables of Spectral Line Intensities (NBS Monograph 145, part I ; Washington: U.S. G.P.O.), 96

Morton, D. C. 2000, ApJS, 130, 403

Nissen, P. E., & Schuster, W. J. 2010, A&A, 511, L10

Pequignot, D., & Baluteau, J.-P. 1994, A&A, 283, 593

Pignatari, M., Gallino, R., Heil, M., et al. 2010, ApJ, 710, 1557

Piskunov, N. E., & Valenti, J. A. 2002, A&A, 385, 1095

Prochaska, J. X., Howk, J. C., & Wolfe, A. M. 2003, Nature, 423, 57

Pwa, T. H., & Pottasch, S. R. 1986, A&A, 164, 116

Raiteri, C. M., Busso, M., Picchio, G., & Gallino, R. 1991, ApJ, 371, 665

Reddy, B. E., Tomkin, J., Lambert, D. L., & Allende Prieto, C. 2003, MNRAS, 340, 304

Reddy, B. E., Lambert, D. L., & Allende Prieto, C. 2006, MNRAS, 367, 1329

Roederer, I. U., Cowan, J. J., Karakas, A. I., et al. 2010, ApJ, 724, 975

Roederer, I. U., & Lawler, J. E. 2012, ApJ, 750, 76

Roederer, I. U., Lawler, J. E., Sobeck, J. S., et al. 2012, ApJS, submitted

Schuster, W. J., Moreno, E., Nissen, P. E., & Pichardo, B. 2012, A&A, 538, A21

Sharpee, B., Zhang, Y., Williams, R., et al. 2007, ApJ, 659, 1265

Simmerer, J., Sneden, C., Cowan, J. J., et al. 2004, ApJ, 617, 1091

Sneden, C. A. 1973, Ph.D. Thesis, Univ. of Texas at Austin

Sneden, C., Cowan, J. J., Burris, D. L., & Truran, J. W. 1998, ApJ, 496, 235

Sneden, C., Cowan, J. J., Lawler, J. E., et al. 2003, ApJ, 591, 936

Sneden, C., Cowan, J. J., & Gallino, R. 2008, ARA&A, 46, 241

Sneden, C., Lawler, J. E., Cowan, J. J., Ivans, I. I., & Den Hartog, E. A. 2009, ApJS, 182, 80

Sobeck, J. S., Kraft, R. P., Sneden, C., et al. 2011, AJ, 141, 175

Sterling, N. C., Dinerstein, H. L., & Bowers, C. W. 2002, ApJ, 578, L55

Sterling, N. C., & Dinerstein, H. L. 2008, ApJS, 174, 158

Travaglio, C., Gallino, R., Arnone, E., et al. 2004a, ApJ, 601, 864

Travaglio, C., Hillebrandt, W., Reinecke, M., & Thielemann, F.-K. 2004b, A&A, 425, 1029

Tomkin, J., Lambert, D. L., Edvardsson, B., Gustafsson, B., & Nissen, P. E. 1989, A&A, 219, L15

Tull, R. G., MacQueen, P. J., Sneden, C., & Lambert, D. L. 1995, PASP, 107, 251

Unsöld, A., Physik der Sternatmosphären, Springer-Verlag, Berlin, 1955, p. 332–333

van Leeuwen, F. 2007, A&A, 474, 653

Venn, K. A., Irwin, M., Shetrone, M. D., et al. 2004, AJ, 128, 1177

Vogt, S. S., Allen, S. L., Bigelow, B. C., et al. 1994, Proc. SPIE, 2198, 362

Wanajo, S., Janka, H.-T., & Müller, B. 2011, ApJ, 726, L15

Wiese, W. L., & Martin, G. A. 1980, Nat. Stand. Ref. Data Ser., Nat. Bur. Stand., U.S., 68, 359

Westin, J., Sneden, C., Gustafsson, B., & Cowan, J. J. 2000, ApJ, 530, 783

Woodgate, B. E., Kimble, R. A., Bowers, C. W., et al. 1998, PASP, 110, 1183

Woolf, V. M., Tomkin, J., & Lambert, D. L. 1995, ApJ, 453, 660